Multicomponent interparticle-potential lattice Boltzmann model for fluids with large viscosity ratios

Mark L. Porter,[1,*] E. T. Coon,[2] Q. Kang,[3] J. D. Moulton,[2] and J. W. Carey[1]
[1]*Earth Systems Observations, EES-14, Los Alamos National Laboratory, Los Alamos, New Mexico, USA*
[2]*Applied Mathematics and Plasma Physics, T-5, Los Alamos National Laboratory, Los Alamos, New Mexico, USA*
[3]*Computational Earth Sciences, EES-16, Los Alamos National Laboratory, Los Alamos, New Mexico, USA*
(Received 18 May 2012; published 10 September 2012)

This work focuses on an improved multicomponent interparticle-potential lattice Boltzmann model. The model results in viscosity-independent equilibrium densities and is capable of simulating kinematic viscosity ratios greater than 1000. External forces are incorporated into the discrete Boltzmann equation, rather than through an equilibrium velocity shift as in the original Shan and Chen (hereafter, SC) model. The model also requires the derivation of a momentum conserving effective velocity, which is substituted into the equilibrium distribution function and applies to both the single- and multiple-relaxation-time formulations. Additionally, higher-order isotropy is used in the calculation of the fluid-fluid interaction forces to reduce the magnitude of spurious currents (i.e., numerical errors) in the vicinity of interfaces. First, we compare the model to the SC model for static bubble simulations. We demonstrate that the model results in viscosity-independent equilibrium bubble densities for a wide range of kinematic viscosities, which is not the case for the SC model. Furthermore, we show that the model is capable of simulating stable bubbles for kinematic viscosity ratios greater than 1000 (when higher-order isotropy is used), whereas the SC model is known to be limited to kinematic viscosity ratios on the order of 10. Next we verify the model for surface tension via Laplace's law and show that the model results in the same surface tension values for a range of kinematic viscosities and kinematic viscosity ratios of 10, 100, and 1000. The model is also verified for layered cocurrent flow though parallel plates. We show that the simulated velocity profiles preserve continuity at the interface for kinematic viscosity ratios ranging from 0.001 to 1000 and that the model accurately predicts nonwetting and wetting phase relative permeability for kinematic viscosity ratios of 0.01 to 100.

DOI: 10.1103/PhysRevE.86.036701 PACS number(s): 47.11.−j, 47.55.Ca

I. INTRODUCTION

The lattice Boltzmann (LB) method has become a promising alternative to traditional computational fluid dynamics (CFD) for simulating complex fluid flows encountered in a variety of engineering applications. This is partly due to the relative ease with which complex boundaries are handled and the method's excellent scaling on parallel processing systems [1,2]. The LB method is particularly attractive for multicomponent and multiphase flows involving interfacial dynamics and phase transitions since it is based on simplified kinetic models. This makes it relatively easy to incorporate underlying microscopic interactions at the interface, bypassing the need for special interfacial treatment commonly required in other CFD methods [1,3,4].

Numerous multicomponent and multiphase LB models have been reported in the literature, all of which fall into four basic categories: the color model [5], the interparticle-potential model [6,7], the free-energy model [8], and the mean-field model [9,10]. A number of reviews have been published describing these models and discussing recent developments [1,2,4,11]. In this work, we focus on the multicomponent interparticle-potential model originally developed by Shan and Chen [6,7] (SC), which is one of the most successful LB models [12,13]. In the SC model, a pairwise interaction force between components (or phases) is introduced that modifies the collision operator through an equilibrium velocity [6,7]. This force includes a parameter controlling the interaction strength that causes phase separation and introduces surface-tension effects when sufficiently large.

Despite its success, the SC model has several limitations including, but not limited to, large spurious currents in the vicinity of the fluid-fluid interface, viscosity-dependent equilibrium densities, numerical instabilities for large density ratios, and numerical instabilities for multicomponent flows with large kinematic viscosity ratios. Recent work has shown that spurious currents are caused by the lack of sufficient isotropy in the calculation of the gradient in the interaction potential, and by adopting a finite difference gradient operator with sufficient spatial isotropy they can be arbitrarily reduced [12,14]. Yu and Fan [15] presented a single-component multiphase model that results in viscosity-independent equilibrium densities; however, this has not been addressed for multicomponent interparticle-potential models. Instabilities for fluids with large density ratios have recently been addressed for single-component systems [16–18] and multicomponent systems [19]. To the best of our knowledge, numerical instabilities encountered in multicomponent flows with large kinematic viscosity ratios have not been addressed in the literature. The ability to simulate a wider range of kinematic viscosity ratios is important for immiscible displacement in porous media. In these systems the value of the dynamic viscosity ratio ($M = \frac{\rho_b \nu_b}{\rho_s \nu_s}$) determines the resulting fluid configurations [21]. In addition, buoyancy forces are often negligible since capillary forces dominate (e.g., Ref. [22]). Thus, a model that can handle a wide range

*porterma@lanl.gov

of kinematic viscosity ratios is important since M can be matched while keeping the density ratio equal to 1. To date, studies using multicomponent interparticle-potential models have been constrained to fluids with kinematic viscosity ratios less than 16 [19,22–29] or maintain a viscosity ratio of 1 and make simplifying assumptions regarding the simulated system [30,31].

In this work, we describe a multicomponent interparticle-potential LB model that simulates viscosity-independent equilibrium densities and kinematic viscosity ratios greater than 1000. Our model, which we call the explicit forcing (EF) model, is similar to the model proposed by Yu *et al.* [20] in that external forces are incorporated into the discrete Boltzmann equation for each component. However, the forcing term in our model differs from the one in the Yu *et al.* [20] model, which we discuss in the next section. In addition, the EF model requires a momentum conserving effective velocity that is substituted into the equilibrium distribution function. The EF model is implemented for both the single- and multiple-relaxation-time (SRT and MRT, respectively) schemes, and we apply higher-order spatial isotropy in the fluid-fluid interaction force to reduce spurious currents in the vicinity of interfaces. We stress that the use of higher-order isotropy enabled us to achieve kinematic viscosity ratios greater than 300 with the EF model. We also note that our implementation is freely available in the open source software TAXILA LBM [32].

The remainder of this manuscript is organized as follows. In Sec. II, we first review the SC model, and then describe higher-order isotropy in the approximation of the fluid-fluid forces. Next, we discuss the theoretical details of the EF model for both SRT and MRT. In Sec. III, we present extensive numerical simulations that verify and highlight features of the improved interparticle-potential model. These include static bubbles for equilibrium densities and surface tension, as well as layered cocurrent flow in a channel to investigate continuity at the interface and relative permeability. The EF model simulations are compared to SC model simulations and analytical solutions. We conclude with a discussion and summary of our findings in Sec. IV.

II. LATTICE BOLTZMANN METHOD

The LB method solves the discrete Boltzmann equation for an ensemble-averaged distribution of particles, $f_i(\mathbf{x},t)$, on a discrete lattice connected by fixed paths. The particles move along the fixed paths at fixed velocities $\mathbf{e}_i$, where i indicates the velocity direction. The set of $\mathbf{e}_i$ is determined by the lattice dimensions and the neighboring lattice sites included in the lattice structure (see Ref. [11] for typical lattice structures). In this study, we use the D2Q9 (two-dimensional nine velocity) square lattice, and we note that the EF model is implemented for the D3Q19 (three-dimensional 19 velocity) lattice in TAXILA LBM [32].

A. Interparticle-potential model

For completeness, we first review the multicomponent interparticle-potential model developed by Shan and Chen [6,7]. In the SC model, k distribution functions are introduced to represent a fluid mixture containing k fluid components. In this work, we focus on binary mixtures (i.e., $k = 2$); however, this formulation, and our implementation, applies to any number of components. In addition, we only consider components with the same molecular mass, but note that the model is easily extended to components with different molecular mass (see Refs. [6,33]). Each distribution function satisfies the discrete Boltzmann equation

$$f_i^k(\mathbf{x} + \mathbf{e}_i \Delta t, t + \Delta t) - f_i^k(\mathbf{x},t) = \Omega_{\text{coll}}^k, \tag{1}$$

where Ω_{coll}^k is the collision operator, which has the form for SRT

$$\Omega_{\text{coll}}^k = \frac{f_i^{\text{eq},k}(\mathbf{x},t) - f_i^k(\mathbf{x},t)}{\tau_k}. \tag{2}$$

The parameter τ_k is the dimensionless relaxation rate for each component that is related to the kinematic viscosity by $\nu_k = (\tau_k - 0.5)/3$. The equilibrium distribution function $f_i^{\text{eq},k}$ is expressed as Ref. [34]

$$f_i^{\text{eq},k} = w_i \rho_k \left[1 + \frac{\mathbf{e}_i \cdot \mathbf{u}_k^{\text{eq}}}{c_s^2} + \frac{\left(\mathbf{e}_i \cdot \mathbf{u}_k^{\text{eq}}\right)^2}{2c_s^4} - \frac{\mathbf{u}_k^{\text{eq}} \cdot \mathbf{u}_k^{\text{eq}}}{2c_s^2} \right], \tag{3}$$

where w_i are weights specific to the chosen lattice (see Ref. [2], Table 1) and $c_s = 1/\sqrt{3}$ is the speed of sound. It is noted that Eq. (3) was obtained via *a posteriori* matching of the macroscopic dynamics using a Chapman-Enskog expansion. It has been shown that Eq. (3) corresponds to the second-order Hermite expansion, and higher-order approximations can be systematically constructed through Hermite expansions [35]. The macroscopic density and momentum of the kth component are defined as

$$\rho_k = \sum_i f_i^k \tag{4}$$

and

$$\rho_k \mathbf{u}_k = \sum_i f_i^k \mathbf{e}_i, \tag{5}$$

respectively. The adjusted momentum for each component, $\mathbf{u}_k^{\text{eq}}$, appearing in Eq. (3) is defined as Refs. [6,7]

$$\rho_k \mathbf{u}_k^{\text{eq}} = \rho_k \mathbf{u}' + \tau_k \mathbf{F}_k, \tag{6}$$

where $\mathbf{u}'$ is an effective velocity and $\mathbf{F}_k$ is the total force (including fluid-fluid interactions) acting on the kth component. To conserve momentum in the absence of forces, $\mathbf{u}'$ must satisfy [6,7]

$$\mathbf{u}' = \sum_k \frac{\rho_k \mathbf{u}_k}{\tau_k} \Big/ \sum_k \frac{\rho_k}{\tau_k}. \tag{7}$$

Briefly, Eq. (7) can be derived by mapping Eq. (2) to moment space for momentum by multiplying by $\mathbf{e}_i$, summing over i and k, and setting the result equal to zero.

In the SC model, a mean-field interaction force models nonlocal molecular interactions among particles, which is expressed as

$$\mathbf{F}_k(\mathbf{x}) = -\psi_k(\mathbf{x}) \sum_{\bar{k}} g_{k\bar{k}} \sum_i \psi_{\bar{k}}(\mathbf{x} + \mathbf{e}_i)\mathbf{e}_i, \tag{8}$$

where ψ_k is the interparticle potential (or "effective mass") that induces proper phase separation and $g_{k\bar{k}}$ is the interaction

strength. Several functional forms of ψ_k have been proposed in the literature [6,7,16,36]; for binary mixtures, $\psi_k = \rho_k$ was used in the original SC model. The interactions within each component, g_{11} and g_{22}, are typically set equal to zero for binary mixtures, whereas the interactions between components, g_{12} $(=g_{21})$, must be sufficiently large to induce phase separation. Thus, g_{12} effectively controls the surface tension and immiscibility of the binary mixture. It should be noted that multicomponent interparticle-potential LB models result in partially miscible fluids. Thus, when modeling immiscible systems it is important to choose g_{12} large enough that the dissolution of one phase into the other is sufficiently small.

B. Higher-order isotropy

In recent works, it has been recognized that the right-hand side of Eq. (8) is the finite difference representation of $-\psi\nabla\psi$ with unspecified interaction strengths at different distances [14,16]. Thus, Eq. (8) can be expressed in potential form as Ref. [16]

$$\mathbf{F}_k(\mathbf{x}) = -c_0\psi_k(\mathbf{x})\sum_{\bar{k}} g_{k\bar{k}}\nabla\psi_{\bar{k}}(\mathbf{x}), \tag{9}$$

where c_0 is a constant depending on the lattice structure ($c_0 = 6$ for the D2Q9 and D3Q19 lattices). With the generalized form of Eq. (9) the finite difference gradient operator can be constructed to include any number of neighbors as long as care is taken to preserve a sufficient degree of isotropy. One of the earlier works to report the use of higher-order isotropy was Falcucci *et al.* [37]. In other works, Shan [14] and Sbragaglia *et al.* [12] provide derivations of the appropriate weights for several isotropy orders in 2D and 3D, and they showed that spurious currents can be reduced in the vicinity of interfaces when the isotropy order is increased. In our code, we have implemented isotropy orders of 4, 8, and 10 in 2D as well as 4 and 8 in 3D, and we have accounted for the presence of arbitrarily shaped solids. An isotropy order of 4 corresponds to evaluating the gradient using the nearest and next-nearest neighbors in both the D2Q9 and D3Q19 lattices [14], which is consistent with the original SC model. In both the SC and EF models we use Eq. (9) for the fluid-fluid interaction force.

Given the interaction force in Eq. (9), the equation of state (EOS) for the system is given by

$$p = c_s^2\sum_k \rho_k + \frac{c_0}{2}\sum_{k\bar{k}} g_{k\bar{k}}\psi_k\psi_{\bar{k}}. \tag{10}$$

If there are no fluid-fluid interaction forces, then the fluid will act as an ideal gas. Different EOSs can be obtained by changing ψ_k. We have set $\psi_k = \rho_k$ for this work, but we note that Van der Walls type EOSs are available in TAXILA LBM [32].

C. Explicit forcing model

In the SC model, momentum adjustments due to external forces are incorporated into the equilibrium velocity [see Eq. (6)]. In the EF model, the forcing term is directly included in the discrete Boltzmann equation for each component. This yields the implicit expression

$$f_i^k(\mathbf{x}+\mathbf{e}_i\Delta t, t+\Delta t) - f_i^k(\mathbf{x},t) = \Omega_{\text{coll}}^k + \frac{\Delta t}{2}\left[f_i^{F,k}(\mathbf{x}+\mathbf{e}_i\Delta t, t+\Delta t) + f_i^{F,k}(\mathbf{x},t)\right], \tag{11}$$

where $f_i^{F,k}$ accounts for changes to the distribution function due to external forces and Ω_{coll}^k is the same as Eq. (2) for SRT. The forcing term is defined as Ref. [9]

$$f_i^{F,k} = \frac{\mathbf{F}_k\cdot(\mathbf{e}_i - \mathbf{u}^{\text{eq}})}{\rho_k c_s^2} f_i^{\text{eq},k}, \tag{12}$$

where $\mathbf{F}_k$ are the external forces. The EF model in this work differs from the model used by Yu *et al.* [20] in that we evaluate all terms in Eq. (12), whereas Yu *et al.* [20] neglect terms that are second order or higher. The equilibrium distribution function $f_i^{\text{eq},k}$ has the same form as Eq. (3), but $\mathbf{u}_k^{\text{eq}}$ is replaced with an effective momentum for the fluid mixture, $\mathbf{u}^{\text{eq}}$, that is equivalent to Eq. (7) (i.e., $\mathbf{u}^{\text{eq}} = \mathbf{u}'$) for the SRT formulation. The momentum substituted into Eq. (3) is different between the two models because of the $\mathbf{F}_k$ treatment. In the SC model, the external forces are introduced to the distribution function through $\mathbf{u}_k^{\text{eq}}$. Thus, $\mathbf{u}_k^{\text{eq}}$ is defined as an effective momentum (independent of a specific component) plus the changes in momentum due to the forces acting on each component, making it component specific. Here, the forces are directly incorporated into the distribution function, thus $\mathbf{u}^{\text{eq}}$ is simply an effective velocity for the fluid mixture.

The transformation $\bar{f}_i^k = f_i^k - \frac{\Delta t}{2} f_i^{F,k}$ [9,38] is applied to Eqs. (2) and (11) to yield an explicit scheme expressed as

$$\bar{f}_i^k(\mathbf{x}+\mathbf{e}_i\Delta t, t+\Delta t) - \bar{f}_i^k(\mathbf{x},t) = \frac{1}{\tau_k}\left[f_i^{\text{eq},k}(\mathbf{x},t) - \bar{f}_i^k(\mathbf{x},t) - \frac{\Delta t}{2} f_i^{F,k}\right] + \Delta t f_i^{F,k}. \tag{13}$$

The macroscopic properties for each component are defined as

$$\rho_k = \sum_i \bar{f}_i^k \tag{14}$$

and

$$\rho_k\mathbf{u}_k = \sum_i \bar{f}_i^k\mathbf{e}_i + \frac{\Delta t}{2}\mathbf{F}_k. \tag{15}$$

Notice that the external forces naturally arise in the definition of the component momentum, which differs from the SC model [see Eq. (5)]. Thus, substitution of Eq. (15) into Eq. (7) indicates that the effective velocity in the proposed model accounts for external forces acting on each fluid component. The total velocity of the fluid mixture is

$$\mathbf{u} = \frac{\sum_k \rho_k\mathbf{u}_k}{\sum_k \rho_k}. \tag{16}$$

D. Multiple-relaxation-time formulation

We now provide details regarding MRT for the EF model. It is noted that many of the developments described in this section stem from the seminal works of Higuera *et al.* [39], Higuera and Jiménez [40], and Benzi *et al.* [41].

In the MRT formulation both Ω_{coll}^k and $\mathbf{u}^{\text{eq}}$ are defined differently than in the SRT formulation. The collision operator is now defined as

$$\Omega_{\text{coll}}^k = \mathbf{T}^{-1}\hat{\Lambda}^k\mathbf{T}\left[f_i^{\text{eq},k}(\mathbf{x},t) - \bar{f}_i^k(\mathbf{x},t)\right], \tag{17}$$

where $\mathbf{T}$ is a transformation matrix and $\hat{\Lambda}^k$ is a diagonal relaxation matrix. For the D2Q9 square lattice, the transformation matrix is defined as [42]

$$\mathbf{T} = \begin{bmatrix} 1 & 1 & 1 & 1 & 1 & 1 & 1 & 1 & 1 \\ -4 & -1 & -1 & -1 & -1 & 2 & 2 & 2 & 2 \\ 4 & -2 & -2 & -2 & -2 & 1 & 1 & 1 & 1 \\ 0 & 1 & 0 & -1 & 0 & 1 & -1 & -1 & 1 \\ 0 & -2 & 0 & 2 & 0 & 1 & -1 & -1 & 1 \\ 0 & 0 & 1 & 0 & -1 & 1 & 1 & -1 & -1 \\ 0 & 0 & -2 & 0 & 2 & 1 & 1 & -1 & -1 \\ 0 & 1 & -1 & 1 & -1 & 0 & 0 & 0 & 0 \\ 0 & 0 & 0 & 0 & 0 & 1 & -1 & 1 & -1 \end{bmatrix}, \tag{18}$$

where each row has physical significance related to the moments of $\bar{f}_i^k$ in discrete velocity space (for details see Refs. [42,43]). The diagonal relaxation matrix is defined as

$$\hat{\Lambda}^k = \mathrm{diag}\left[s_c^k, s_e^k, s_\varepsilon^k, s_c^k, s_q^k, s_c^k, s_q^k, s_\nu^k, s_\nu^k\right], \tag{19}$$

where s_i^k are the relaxation rates for each $\bar{f}_i^k$. The relaxation parameter s_c^k corresponds to the conserved moments (i.e., density and momentum) and should be nonzero [43], whereas s_e^k, s_ε^k, s_q^k, and s_ν^k correspond to the nonconserved moments (energy, energy squared, energy flux, and stress tensor, respectively). In this formulation, s_e^k, s_ε^k, and s_q^k are free parameters and $s_\nu^k = 1/\tau_k$. It is noted that if all s_i^k in Eq. (19) are set to $1/\tau_k$, then the MRT formulation reduces to SRT. For details regarding $\mathbf{T}$ and $\hat{\Lambda}^k$ for the D3Q19 lattice, see D'Humières *et al.* [44] and Premnath and Abraham [45].

In order to ensure that the EF model conserves momentum in the absence of forces (i.e., $\mathbf{F}_k = 0$), $\mathbf{u}^{\mathrm{eq}}$ must be derived for the MRT formulation. In this case, the collision operator is defined by Eq. (17) and we observe that rows 4 and 6 of $\mathbf{T}$ map $\bar{f}_i^k$ to the x and y components of the kth-component's momentum. Thus, to conserve momentum in the absence of forces, we consider the following:

$$\left(\mathbf{T}\left[\sum_k \mathbf{T}^{-1}\hat{\Lambda}^k\mathbf{T}\left[f_i^{\mathrm{eq},k}(\mathbf{x},t) - \bar{f}_i^k(\mathbf{x},t)\right]\right]\right)_{4,6} = \mathbf{0}. \tag{20}$$

As $\mathbf{T}$ is independent of k and noting that $\hat{\Lambda}_4^k = \hat{\Lambda}_6^k = s_c^k$, we have

$$\sum_k s_c^k \mathbf{T}_{4,6}\left[f_i^{\mathrm{eq},k}(\mathbf{x},t) - \bar{f}_i^k(\mathbf{x},t)\right] = \mathbf{0}, \tag{21}$$

or equivalently

$$\sum_k s_c^k \sum_i \mathbf{e}_i\left[f_i^{\mathrm{eq},k}(\mathbf{x},t) - \bar{f}_i^k(\mathbf{x},t)\right] = \mathbf{0}. \tag{22}$$

Thus, an appropriate definition for $\mathbf{u}^{\mathrm{eq}}$ that conserves momentum is

$$\mathbf{u}^{\mathrm{eq}} = \sum_k s_c^k \rho_k \mathbf{u}_k \Big/ \sum_k s_c^k \rho_k. \tag{23}$$

Note that Eq. (23) reduces to Eq. (7) when $s_c^k = 1/\tau_k$ and $\mathbf{u}^{\mathrm{eq}} = \mathbf{u}$ [Eq. (16)] when $s_c^k = 1$. Furthermore, Eq. (23) can easily be extended to 3D by considering the terms associated with the momentum in $\hat{\Lambda}^k$ for the D3Q19 lattice.

III. NUMERICAL RESULTS AND DISCUSSION

To verify the EF model, we conduct numerical simulations for static bubbles and layered cocurrent flow between two parallel plates for several fluid systems. For the static bubble simulations we compare EF model results with simulation results from the SC model and verify the EF model with Laplace's law. For layered cocurrent flow, we compare EF model simulations to analytical solutions for the velocity profiles and relative permeability curves.

A. Static bubbles

Static bubble simulations consist of initializing a spherical bubble of one fluid located at the center of a domain containing a different suspending fluid. Periodic boundary conditions are applied on all boundaries and the system is allowed to relax to equilibrium. We are interested in the kinematic viscosity ratio ν_b/ν_s, where the subscripts b and s refer to the bubble and suspending fluids, respectively. First we compare simulation results between the two models for 2D static bubbles, in which the kinematic viscosity ratio is 1 and ν_b has values from 0.03 to 0.37. The radius of the bubble is $R = 24$ and it is placed within a suspending fluid domain of 62×62 lattice sites. The interaction strength between components is $g_{12} = g_{21} = 0.17$, which produces sufficient phase separation. In addition, we used the SRT formulation and set the isotropy order to 4 to be consistent with the original formulation of the SC model. Figure 1 compares the bubble density ρ_b and the maximum magnitude of the spurious currents $|\mathbf{u}_s|$ obtained from the SC and EF models. The SC model results in a bubble density that is dependent on the chosen viscosity, whereas the EF model results in a bubble density that is independent of viscosity. In addition, the spurious currents are reduced by almost two orders of magnitude with the EF model. Overall, Fig. 1 shows considerable improvement with the EF model as compared to the SC model for static bubbles with a kinematic viscosity ratio of 1.

Next we consider static bubble simulations for kinematic viscosity ratios greater than 1. With the SC model we obtained stable results up to $\nu_b/\nu_s = 5$. This is consistent with

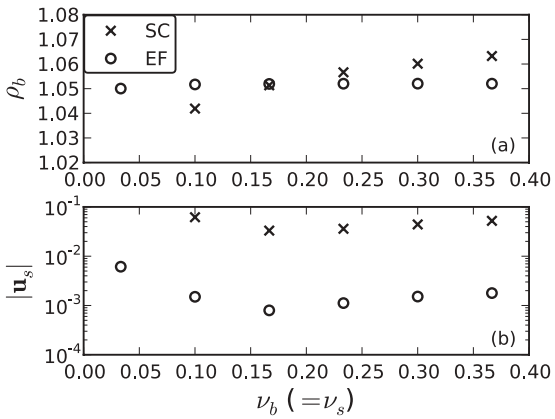

FIG. 1. Comparison between the SC and EF models of (a) bubble density and (b) magnitude of spurious currents for static bubble simulations consisting of several viscosities and a kinematic viscosity ratio of 1.

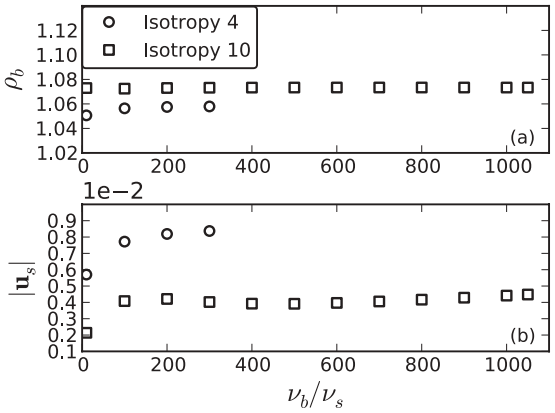

FIG. 2. Comparison of (a) bubble density and (b) magnitude of spurious currents resulting from static bubble simulations using the EF model with isotropy orders of 4 and 10.

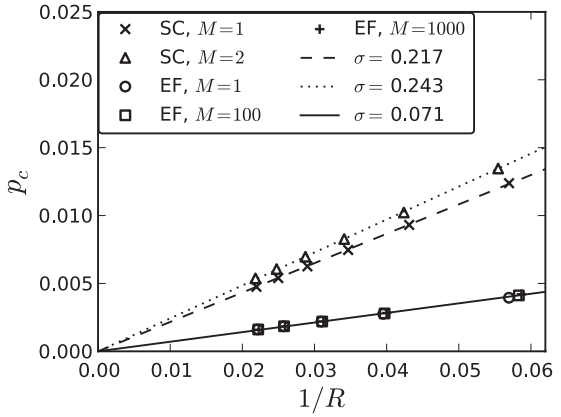

FIG. 3. Verification of Laplace's law for the SC and EF models. The lines represent least-square-fit lines to the simulation results.

previously published results [28,29], thus they are not shown here. It is also noted that, in order to obtain stable bubbles for higher kinematic viscosity ratios with the SC model, g_{12} had to be reduced, which resulted in greater miscibility between the two fluids. For the EF simulations a bubble with $R = 24$ is placed within a suspending fluid domain of 62×62 lattice sites and the interaction strength between components is $g_{12} = g_{21} = 0.17$. The viscosity of the suspending fluid is $\nu_s = 0.0067$, whereas the viscosity of the bubble is varied to achieve different kinematic viscosity ratios. We ran two sets of simulations, one using an isotropy order of 4 and the other using an isotropy order of 10. Both sets of simulations were run with the SRT formulation. Figure 2 shows the bubble densities and magnitude of spurious currents resulting from the EF model using the two different isotropy orders. The isotropy 4 simulations result in stable bubbles up to $\nu_b/\nu_s = 300$, whereas the isotropy 10 simulations result in stable bubbles for ν_b/ν_s up to 1050. This is a viscosity ratio that is more than two orders of magnitude greater than the SC model can simulate. The increased stability of the isotropy 10 simulations is a direct result of the reduction in $|\mathbf{u}_s|$, which is approximately a factor of 2 for all values of ν_b/ν_s. There is clearly a jump in $|\mathbf{u}_s|$ going from $\nu_b/\nu_s = 10$ to $\nu_b/\nu_s > 100$ for both isotropy orders. In the isotropy 4 simulations, this causes a small difference in ρ_b, however in the isotropy 10 simulations there is no significant difference in ρ_b for all values of ν_b/ν_s. In addition, there is an increase in ρ_b by approximately 1.65% for the isotropy 10 simulations as compared to the isotropy 4 simulations. These differences in ρ_b are again caused by the differences in $|\mathbf{u}_s|$, which are numerical errors that occur in the vicinity of the interface.

We now verify the EF model for surface tension via Laplace's law and compare the results to those obtained with the SC model. According to Laplace's law, the capillary pressure, p_c, for a 2D bubble at equilibrium is defined as

$$p_c = p_b - p_s = \frac{\sigma}{R}, \tag{24}$$

where σ is the surface tension, R is the radius (or curvature) of the bubble, and p_b and p_s are the bubble and suspending fluid pressures, respectively. These simulations are the same as the isotropy order 10 simulations described above, except that R ranges from 18 to 46 lattice sites and is placed in the center of a 121×121 lattice domain. Figure 3 shows the simulation results along with the least-square-fit lines, the slopes of which correspond to the surface tension. It can be seen that both models obey Laplace's law as demonstrated by the least-square-fit lines. However, the EF model obtains practically identical surface tensions for $\nu_b/\nu_s = 1$, $\nu_b/\nu_s = 100$, and $\nu_b/\nu_s = 1000$, whereas the SC model surface tension is clearly dependent upon the kinematic viscosity ratio. It is noted that the SC model results shown in Fig. 3 are consistent with those published by Dong *et al.* (Ref. [29], Fig. 1) for viscosity ratios ranging from 1 to 5. In addition, the EF model results in a reduction of surface tension by a factor of approximately 3 compared to the SC model, which is largely due to the reduction in $|\mathbf{u}_s|$ in the EF model. One implication of the reduced spurious currents and surface tension is that the improved model can achieve a wider range of capillary numbers in the simulation of multicomponent fluids than the original SC model.

The results presented thus far suggest that with the EF model there is a unique relationship between surface tension and the interaction strength g_{12} that is independent of the chosen viscosity and viscosity ratio. Thus, we conducted a series of static bubble simulations each with a radius of $R = 43$ in a domain that is 121×121 lattice sites, and varied g_{12} for kinematic viscosities ranging from 0.17 to 1.5. The results of these simulations are presented in Fig. 4 along with those from the SC model for viscosities of 0.17 and 0.5. Clearly, the surface tension from the EF model shows very little dependence upon the viscosity (especially for small g_{12} values), whereas the SC model shows a strong dependence. Thus, a simple quadratic fit ($\sigma = -1.361 g_{12}^2 + 1.721 g_{12} - 0.178$) can be used as a tool to estimate surface tension for a given g_{12} for any viscosity with the EF model. This greatly decreases the computational cost and effort when using multicomponent interparticle-potential LB models since the EF model bypasses the need to run static bubble simulations for every fluid pair of interest, which has been a drawback of the SC model.

B. Two-phase cocurrent flow

In order to test the EF model under steady state, laminar flow conditions, we consider two-phase cocurrent flow between

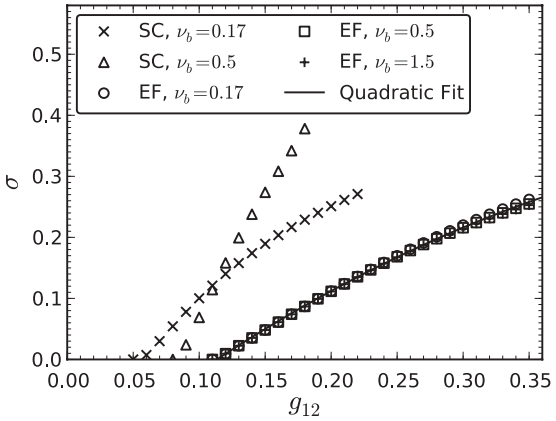

FIG. 4. Surface tension as a function of g_{12} for different viscosity values ($M = 1$).

two parallel plates. In this system, the wetting phase flows between the nonwetting phase and the wall, whereas the nonwetting phase flows between the wetting phase only and does not contact the wall. A schematic of the system along with the analytical solution for the velocity profile and relative permeability of each phase is provided in the Appendix. It is noted that the analytical solution for the nonwetting phase relative permeability [Eq. (A5)] is a function of the dynamic viscosity ratio $M = \frac{\rho_b \nu_b}{\rho_s \nu_s}$. Thus, in this section we will refer to the viscosity ratio as M, but it is stressed that in all cases the density ratio is 1 and M simplifies to the kinematic viscosity ratio. A body force F_b is applied to both fluids to induce flow. Periodic boundaries are applied at the inlet and outlet and bounce-back boundary conditions are applied at the walls. We conduct simulations for $0.001 \leqslant M \leqslant 1000$, in which the smallest viscosity was 3.33×10^{-4} and the largest viscosity was 1.5 to cover the range of kinematic viscosity ratios. We stress that MRT and higher-order isotropy of 10 was required for the $M = 0.001$ and $M = 1000$ simulations to preserve continuity at the interface. Figure 5 shows the comparison between the velocity profiles for the analytical solution [Eqs. (A1) and (A2)] and the EF model. The velocity profiles have been normalized by the maximum analytical velocity $\hat{u}$ for each value of M. There is good agreement between the EF model simulations and the analytical solution for each value of M, as indicated by the root-mean-squared error, which ranges from 3.18×10^{-3} to 9.85×10^{-3}. In all cases, the largest error occurs at the interface between the two fluids. For $0.1 \leqslant M \leqslant 1000$ the maximum relative percent error is less than 2.5%. For $M = 0.01$ and $M = 0.001$ the maximum relative percent error is approximately 26%, however, this does not have a significant affect on the simulated velocity profile away from the interface. Thus, it can be concluded that continuity at the interface is preserved with the EF model. This is a considerable improvement over most multicomponent LB models that have been used to address this problem, with the notable exception of Ginzburg [46], who used the color model and a two-relaxation-time (TRT) model to obtain continuity at the interface for kinematic viscosity ratios up to 1000. Kang *et al.* [25] and Rannou [47] reported discontinuities at the interface for kinematic viscosity ratios of 3 and 0.08, respectively, using the interparticle-potential

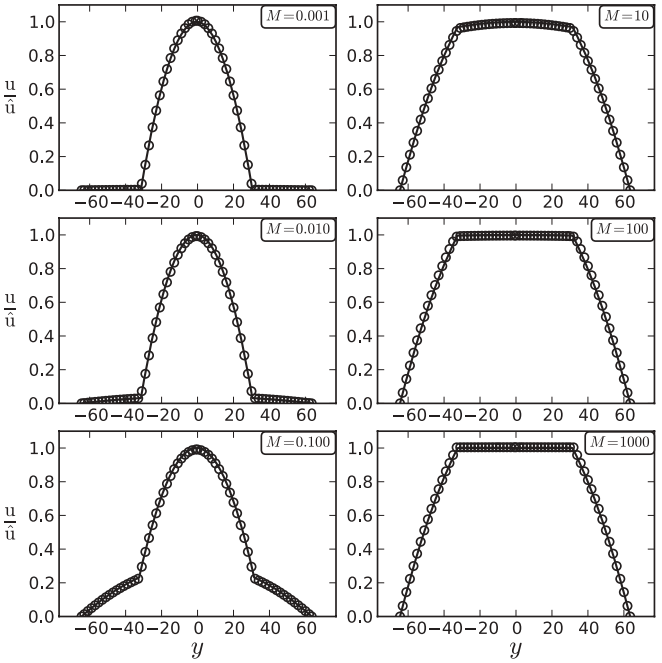

FIG. 5. Simulated (symbols) and analytical (lines) velocity profiles for cocurrent two-phase flow between parallel plates for $0.001 < M < 1000$. In each case, the velocities are normalized by the maximum analytical velocity $\hat{u}$.

model. Moreover, Rannou [47] observed considerable mixing between the fluids when the kinematic viscosity was not 1, which was not observed in our simulations with the EF model. Rannou [47] also showed discontinuities at the interface for both the free-energy model and the mean-field model for kinematic viscosities of 0.01 and 0.052, respectively. In both cases the discontinuity caused significant discrepancies with the analytical solution for one of the fluids and not the other. For all cases in Fig. 5, g_{12} was chosen such that the interface thickness was approximately 4 pixels, which is close to the smallest attainable interface thickness for the EF model in this system. Simulations with larger interface thicknesses (i.e., smaller g_{12} values) showed notable discrepancies with the analytical solution. This is to be expected since the analytical solution assumes a sharp interface and smaller g_{12} values lead to thicker interfaces.

We now present EF simulations for the relative permeability of each phase [Eqs. (A5) and (A6)] as a function of the wetting phase saturation, $S_w = 1 - a/L$ (see Fig. 7), in which we vary a to obtain different S_w values. The nonwetting and wetting phase relative permeability for the EF simulations is calculated using Eqs. (A3) and (A4), respectively. Results for $0.01 \leqslant M \leqslant 100$ using MRT and an isotropy order of 10 are shown in Fig. 6, and the root-mean-squared error and maximum relative percent error are provided in Table I. Overall, the simulations agree well with the analytical solutions for all cases. The most notable errors are exhibited in the $M = 100$ simulations for $k_{r,n}$ corresponding to S_w between 0.25 and 0.50. This can be explained by considering the size of the region occupied by the nonwetting phase for $S_w < 0.50$ and the velocity profile within this region, which is relatively constant (see Fig. 5). For $S_w < 0.50$ the nonwetting phase region is larger than that

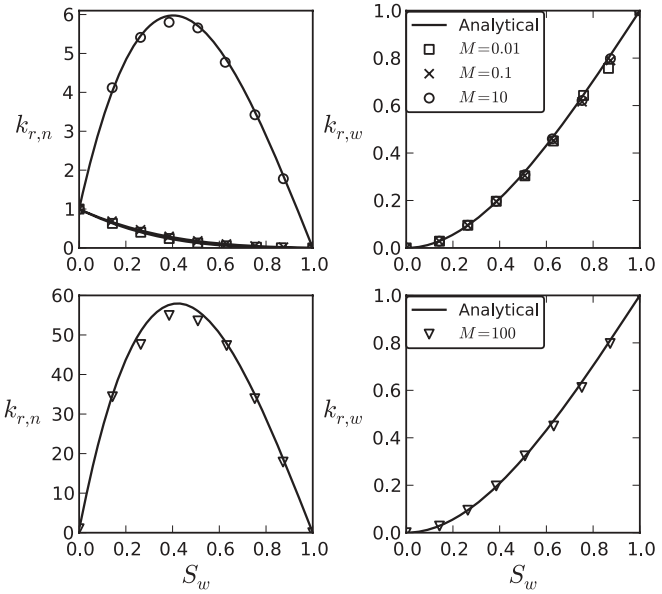

FIG. 6. Comparison between the EF simulations and the analytical solution for the nonwetting (left) and wetting (right) phase relative permeability for cocurrent flow between two parallel plates. The results for $M = 100$ are plotted separately due to the difference in scale for $k_{r,n}$.

for $S_w > 0.50$, thus any discrepancies in the nonwetting phase velocity for simulations corresponding to $S_w < 0.50$ have a more profound affect on the relative permeability estimate than for $S_w > 0.50$. We also found that using MRT and an isotropy order greater than 4 significantly improved the $k_{r,n}$ estimates for $S_w < 0.50$. We expect this to be important for accurate predictions of $k_{r,n}$ in real porous media since grid resolution within the pores is often coarse for sufficiently large porous media samples.

IV. CONCLUSIONS

In this work, we demonstrated that the explicit forcing model is superior to the original SC model for static bubble simulations and layered cocurrent flow between two parallel plates, in that it is capable of simulating fluid pairs with larger kinematic viscosity ratios. The ability to simulate large kinematic viscosity ratios largely results from (1) the treatment of the external forces, which eliminates the unphysical dependence of density on the chosen viscosity; and (2) the use of higher-order isotropy in the evaluation of the fluid-fluid forces, which reduces the magnitude of spurious currents in the vicinity of the interface. In addition, for the layered flow simulations, we found that we also need to use the MRT formulation to further reduce the magnitude of spurious currents in the vicinity of the interface. The combination of all of these features results in a much more stable model that allows us to achieve the large kinematic viscosity ratios.

We also showed that the surface tension is not a function of the viscosity and that a simple quadratic function can be used to estimate surface tension for a given interaction strength, bypassing the need for additional static bubble simulations, which is required when using the original SC model. For layered cocurrent flow, we showed that the velocity profiles simulated with this model preserve continuity at the interface for viscosity ratios ranging from 0.001 to 1000, and that it results in accurate predictions of relative permeability for both phases for viscosity ratios raging from 0.01 to 100.

Overall, the model formulation presented here is more stable, has smaller spurious currents near interfaces, and can simulate a wider range of fluid pairs and flow conditions than the original SC model. It is expected that this model formulation will extend the applicability of multicomponent interparticle-potential LB models to more realistic and complex multicomponent fluid systems; especially for systems involving complex porous media, which will be addressed in future work. As a final note, an implementation of the model is freely available through the open source software TAXILA LBM [32].

TABLE I. The root-mean-squared error (RMSE) and the maximum relative percent error (MRPE) for the relative permeability simulations presented in Fig. 6.

	RMSE		MRPE (%)	
M	$k_{r,n}$	$k_{r,w}$	$k_{r,n}$	$k_{r,w}$
0.01	0.002	0.017	6.6	5.4
0.1	0.010	0.013	3.7	5.1
10	0.086	0.008	4.4	3.9
100	1.73	0.012	6.6	4.8

ACKNOWLEDGMENTS

This work was supported by a grant (No. 20100025DR) through the LDRD-DR program at Los Alamos National Laboratory.

APPENDIX: LAYERED COCURRENT FLOW

For completeness we provide a schematic of the layered co-current flow system along with the analytical solution for the velocity profile and relative permeability of each phase. The system under consideration is shown in Fig. 7 where the wetting fluid flows along the walls ($a \leqslant |y| \leqslant L$) and the nonwetting fluid flows between the wetting phase ($0 \leqslant |y| \leqslant a$). We are interested in the velocity profile perpendicular to the direction of flow. Assuming laminar flow, the analytical

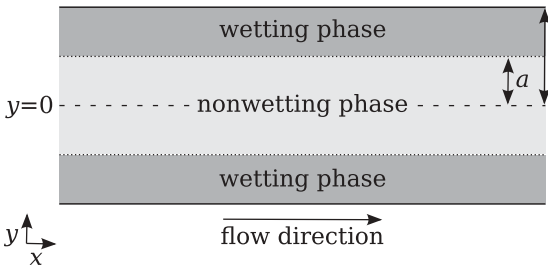

FIG. 7. Schematic of the two-phase cocurrent flow between two parallel plates.

solution for the velocity profile in this system is

$$u(y) = \frac{F_b}{2\nu_n\rho_n}(a^2 - y^2) + \frac{F_b}{2\nu_w\rho_w}(L^2 - a^2), \quad 0 \leqslant |y| \leqslant a, \tag{A1}$$

$$u(y) = \frac{F_b}{2\nu_w\rho_w}(L^2 - y^2), \quad a \leqslant |y| \leqslant L, \tag{A2}$$

where F_b is the body force and the subscripts n and w refer to the nonwetting and wetting phase, respectively. In this work, we apply the same body force to both fluids and the dynamic viscosity ratio produces different average velocities within each phase. The relative permeability of each phase is defined as the ratio of the volumetric flow rate of that phase within the region it occupies during two-phase flow and the volumetric flow rate of that phase over the whole domain during single-phase flow, which is expressed as

$$k_{r,n}(S_w) = \frac{\int_{|y|=0}^{a} u_n\, dy}{\int_{|y|=0}^{L} u_n\, dy}, \tag{A3}$$

$$k_{r,w}(S_w) = \frac{\int_{|y|=a}^{L} u_w\, dy}{\int_{|y|=0}^{L} u_w\, dy}, \tag{A4}$$

where $k_{r,n}$ and $k_{r,w}$ represent the relative permeabilities for the nonwetting and wetting phases, respectively. The analytical solution for the relative permeability of each phase as a function of S_w and M is expressed as [48]

$$k_{r,n} = (1 - Sw)\left[\tfrac{3}{2}M + (1 - S_w)^2\left(1 - \tfrac{3}{2}M\right)\right]. \tag{A5}$$

$$k_{r,w} = \tfrac{1}{2}S_w^2(3 - S_w), \tag{A6}$$

Equations (A5) and (A6) show that $k_{r,n}$ is a function of both S_w and M, whereas $k_{r,w}$ is a function of S_w only.

[1] S. Chen and G. Doolen, Annu. Rev. Fluid. Mech. **30**, 036705 (1998).
[2] C. K. Aidun and J. R. Clausen, Annu. Rev. Fluid. Mech. **42**, 439 (2010).
[3] X. Shan and G. Doolen, Phys. Rev. E **54**, 3614 (1996).
[4] J. Zhang, Microfluid Nanofluid **10**, 1 (2011).
[5] A. K. Gunstensen, D. H. Rothman, S. Zaleski, and G. Zanetti, Phys. Rev. A **43**, 4320 (1991).
[6] X. Shan and H. Chen, Phys. Rev. E **47**, 1815 (1993).
[7] X. Shan and H. Chen, Phys. Rev. E **49**, 2941 (1994).
[8] M. R. Swift, E. Orlandini, W. R. Osborn, and J. M. Yeomans, Phys. Rev. E **54**, 5041 (1996).
[9] X. He, S. Chen, and G. D. Doolen, J. Comput. Phys. **146**, 282 (1998).
[10] J. Zhang, B. Li, and D. Y. Kwok, Phys. Rev. E **69**, 032602 (2004).
[11] R. Nourgaliev, T. Dinh, T. Theofanous, and D. Joseph, Int. J. Multiphase Flow **29**, 117 (2003).
[12] M. Sbragaglia, R. Benzi, L. Biferale, S. Succi, K. Sugiyama, and F. Toschi, Phys. Rev. E **75**, 026702 (2007).
[13] S. Chibbaro, G. Falcucci, G. Chiatti, H. Chen, X. Shan, and S. Succi, Phys. Rev. E **77**, 036705 (2008).
[14] X. Shan, Phys. Rev. E **73**, 047701 (2006).
[15] Z. Yu and L.-S. Fan, Phys. Rev. E **82**, 046708 (2010).
[16] P. Yuan and L. Schaefer, Phys. Fluids **18**, 042101 (2006).
[17] G. Falcucci, S. Ubertini, and S. Succi, Soft Matter **6**, 4357 (2010).
[18] C. Colosqui, G. Falcucci, S. Ubertini, and S. Succi, Soft Matter **8**, 3798 (2012).
[19] S. Chibbaro, Eur. Phys. J. E **27**, 99 (2008).
[20] Z. Yu, H. Yang, and L.-S. Fan, Chem. Eng. Sci. **66**, 3441 (2011).
[21] R. Lenormand, E. Touboul, and C. Zarcone, J. Fluid Mech. **189**, 165 (1988).
[22] C. Pan, M. Hilpert, and C. T. Miller, Water Resources Res. **40**, W01501 (2004).
[23] J. Chin, E. S. Boek, and P. V. Coveney, Philos. Trans. R. Soc. London, Ser. A **360**, 547 (2002).
[24] Q. Kang, D. Zhang, and S. Chen, Phys. Fluids. **14**, 3203 (2002).
[25] Q. Kang, D. Zhang, and S. Chen, Adv. Water Resoures **27**, 13 (2004).
[26] Q. Kang, D. Zhang, and S. Chen, J. Fluid Mech. **545**, 41 (2005).
[27] H. Li, C. Pan, and C. T. Miller, Phys Rev. E **72**, 026705 (2005).
[28] B. Dong, Y. Yan, W. Li, and Y. Song, Comput. Fluids **39**, 768 (2010).
[29] B. Dong, Y. Yan, and W. Li, Transport Porous Med. **88**, 293 (2011).
[30] M. G. Schaap, M. L. Porter, B. S. Christensen, and D. Wildenschild, Water Resources Res. **43**, W12S06 (2007).
[31] M. L. Porter, M. G. Schaap, and D. Wildenschild, Adv. Water Resources **32**, 1632 (2009).
[32] E. T. Coon, M. L. Porter, and Q. Kang, https://software.lanl.gov/taxila
[33] X. Shan, Phys. Rev. E **81**, 045701(R) (2010).
[34] Y. Qian, D. D'Humières, and P. Lallemand, Europhys Lett. **17**, 479 (1992).
[35] X. Shan, X. Yuan, and H. Chen, J. Fluid Mech. **550**, 413 (2006).
[36] N. S. Martys and H. Chen, Phys. Rev. E **53**, 743 (1996).
[37] G. Falcucci, G. Bella, G. Chiatti, S. Chibbaro, M. Sbragaglia, and S. Succi, Commun. Comput. Phys. **2**, 1071 (2007).
[38] X. He, X. Shan, and G. D. Doolen, Phys. Rev. E **57**, R13 (1998).
[39] F. Higuera, S. Succi, and R. Benzi, Europhys. Lett. **9**, 345 (1989).
[40] F. Higuera and J. Jiménez, Europhys. Lett. **9**, 663 (1989).
[41] R. Benzi, S. Succi, and M. Vergassola, Phys. Rep. **222**, 145 (1992).
[42] P. Lallemand and L.-S. Luo, Phys. Rev. E **61**, 6546 (2000).
[43] M. E. McCracken and J. Abraham, Phys. Rev. E **71**, 036701 (2005).
[44] D. D'Humières, I. Ginzburg, M. Krafczyk, P. Lallemand, and L.-S. Luo, Philos. Trans. R. Soc. London, Ser. A **360**, 437 (2002).
[45] K. N. Premnath and J. Abraham, J. Comput. Phys. **224**, 539 (2007).
[46] I. Ginzburg, J. Stat. Phys. **126**, 157 (2007).
[47] G. Rannou, Master's thesis, Geoergia Institute of Technology, 2008.
[48] A. G. Yiotis, J. Psihigios, M. E. Kainourgiakis, A. Papaioannou, and A. K. Stubos, Colloids Surf. A **300**, 35 (2007).